# OPTIMIZATION OF OPEN MICRO-CHANNEL HEAT SINK WITH PIN FINS BY MULTI-OBJECTIVE GENETIC ALGORITHM

by

***Meixia JIANG and Zhongliang PAN****

School of Physics and Telecommunications Engineering,
South China Normal University, Guangzhou, China

Original scientific paper
https://doi.org/10.2298/TSCI211023015J

*Micro-channel heat sink is an effective way to solve the heat dissipation problem of electronic devices because of its compact structure and outstanding heat dissipation ability. In order to obtain the high efficiency and low resistance micro-channel heat sink, a new structure of open rectangular micro-channel heat sink with pin fins was proposed to enhance heat transfer. The orthogonal test method was used to design the experiment, and the 3-D software SOLIDWORKS was used to establish 25 groups of open rectangular micro-channel heat sink with pin fins structure model which has different structural parameters. The numerical calculation was carried out with ANSYS FLUENT simulation software and the experimental values with the structural parameters of the micro-channel heat sink as variables were obtained. According to the simulated experimental values, the objective functions of thermal resistance and pumping power were constructed, and the agent model between objective functions and the optimization variables were established. The Pareto optimal solutions of objective functions were calculated by non-dominated sorting genetic algorithm, which was analyzed by k-means clustering analysis and five clustering points were obtained, and five clusters points were compared and verified by simulation. it was found that there was effective tradeoff points between the highest and lowest points of the five clustering which can make both the pumping power and thermal resistance within the optimal range, so as to obtain the optimal micro-channel heat sink.*

Key words: *micro-channel heat sink, multi-objective optimization, pumping power, thermal resistance, thermal performance*

## Introduction

With the development of micromachining technology, micro-channel heat sink structure has been widely used in the thermal optimization design of 3-D integrated circuits [1-4]. According to the theory of convection heat transfer in micro-channel, the heat transfer performance of micro-channel heat sink can be improved by increasing the heat transfer surface area of the micro-channel heat sink or improving the heat transfer performance of the fluid [5-8]. Chai *et al.* [9] and Xia *et al.* [10] showed that micro-channel heat sink with fan-shaped and triangular cavities can destroy micro-channel flow and heat transfer boundary-layers, which can effectively enhance the heat transfer performance of micro-channels. Hong *et al.* [11] proposed laminar forced convection of water in offset strip-fin micro-channels network heat sinks for microelectronic cooling. It was found that there was an optimal strip-fin size

* Corresponding author, e-mail: panzhongliang@m.scnu.edu.cn

to minimize the pressure drop or pumping power on the constraint condition of maximum wall temperature, and optimal size can depend on the input heat flux and maximum wall temperature. Yadav *et al.* [12] successively carried out optimization of extended surface micro-channel following univariate search method for number of fins, pitch, diameter and height of fins. Bhandari *et al.* [13] studied the heat transfer and fluid-flow characteristics of open micro-channel heat sink consist of pin fins. It was found that heat transfer rate was affected by increasing the height of the fin. Best heat transfer effect was found for the fin height of 1.5 mm. The studies discussed previously emphasize that micro-channel heat sink with pin fins has obvious advantages in improving heat transfer performance.

Reasonable design of micro-channel heat sink can effectively improve heat transfer performance. Heat transfer efficiency and pressure drop are important indexes to measure the heat transfer performance of micro-channel heat sink. In many fields of engineering applications, micro-channel heat sink can be effectively optimized by numerical calculation methods. Husain *et al*. [14] established a 3-D heat transfer model and analyzed the optimal size of micro-channel heat sink. Adham *et al*. [15] proposed an optimization scheme which was applied a systematic thermal resistance model as an analysis method and the elitist non-dominated sorting genetic algorithm. The optimized results showed that the increase in the particles volume fraction results in a decrease in the total thermal resistance and an increase in the pumping power. Vinoth *et al*. [16] researched the heat transfer and flow characteristics of an oblique finned micro-channel heat sink with different inlet cross-sections. The result showed that the oblique finned micro-channel heat sink with the trapezoidal cross-section is suitable for the micro-electronic cooling systems. Kulkarni *et al*. [17] performed that multi-objective optimization of a micro-channel heat sink with a rectangular wedge-shaped cross-section. Two geometric variables related to the channel cross-section and a ratio of flow rates in the upper and lower channels were selected as design variables for the optimization. Thermal resistance and pumping power were considered as objective functions which were obtained by response surface methodology. Multi-objective genetic algorithm was used for optimization, and then the heat transfer effect has been significantly improved.

In this paper, a multi-objective optimization using orthogonal test method, non-dominated sorting genetic algorithm (NSGA-II), and *k*-mean clustering was performed to obtain a Pareto front, with the aim to obtain excellent thermal performance. Twenty five groups of experimental data of open rectangular micro-channel heat sink with pin fins structure models which have different structural parameters were used to optimize design variables ($W_h$, $W_f$, $H_1$-$H_4$) of objective functions (thermal resistance, $R_t$, and pumping power, $P_P$). Five representative solutions obtained by *k*-means clustering, and then through simulation verification and comparison obtain the optimal combination of structural design parameters, making the objective function both $R_t$ and $P_P$ within the optimal range, so as to obtain the optimal heat sink structure.

## Micro-channel heat sink model

### *Micro-channel heat sink structure and description*

Bhandari *et al.* [13] proposed the open rectangular micro-channel heat sink with pin fins as the reference channel design, and multi-objective optimization of structural parameters was carried out. Figures 1(a)-1(c) shows the schematic of the proposed open rectangular micro-channel heat sink with pin fins. Figure 1(a) shows the composition of an open rectangular micro-channel heat sink with pin fins, where $H_c$ is the height of the micro-channel heat sink. Parameters $H_1$-$H_4$ are the heights and $W_f$ and $W_h$ are the length and width of the pin fins in the micro-channel heat sink, respectively. Consequently, there is an open space between the top

surface and the cover plate of the micro-channel heat sink. It is understood that shorter pin fins heights result in more open space available and vice versa. In this structure, coolant flow occurs through channel section as well as open space. Due to this flow amalgamation, pin fins may be completely submerged in the coolant where the top surface of the pin fins also participates in heat transfer process. As reported by Prajapati *et al.* [18], open rectangular micro-channel heat sinks have the advantages of less material requirements for its production, lighter in weight and ease of assembling compared to completely closed ones.

As shown in fig. 1(c), 2 mm adiabatic plenum is set in front of the heating section, with the intention slow down the disturbance caused by the impact fluid jet and enabling avoiding even distribution of the flow into each channel. The matrix material of micro-channel heat sink is copper, and the length, $L$, width, $W$, and height, $H$, of micro-channel heat sink are 27 mm, 10 mm, and 3 mm, respectively. It is composed of a series of pin fins with different fin heights and fin cross-sectional areas. Inline arrangement of four rows of pin fins has been considered with 12 fins in each row as shown in fig. 1(b). The pin fins height of each column is the same, while their heights in different columns can be the same or different. The cross-sectional area of all pin fins were the same. Hence, the total of 48 pin fins of the same cross-sectional area were placed at equal distances from all sides (transverse and lateral). It should be noted that liquid coolant flows in an open area between two side walls having the thickness of 0.5 mm. As mentioned previously, a series of open rectangular micro-channel heat sinks with different pin fins height and cross-sectional areas were designed to find the most appropriate configuration. Table 1 shows the detail dimensions of the considered geometries.

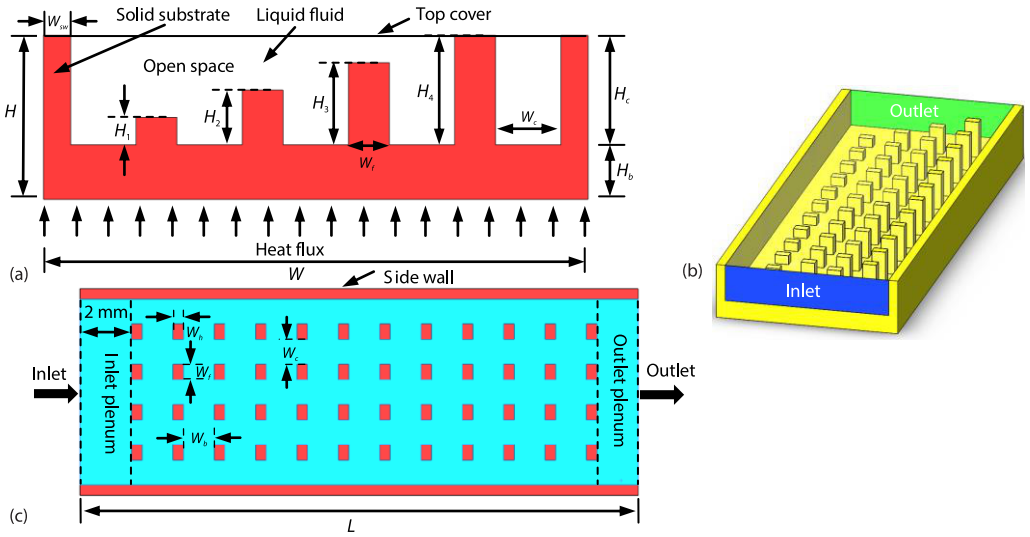


**Figure 1. Schematic of proposed open rectangular micro-channel heat sink with pin fins; (a) cross-sectional view, (b) isometric view, and (c) top view**

## *Model calculation and processing*

The fluid-flow and heat transfer process should follow certain governing equations, including equations of continuity eq. (1), momentum eq. (2), and energy eq. (3), respectively:

$$\nabla\left(\rho_{\mathrm{f}}\vec{\mathrm{V}}\right)=0 \tag{1}$$

**Table 1. Dimensional parameter of micro-channel heat sink**

| Parameter | Value [mm] | Parameter | Value [mm] |
|---|---|---|---|
| Heat sink length, $L$ | 27 | Bottom wall thickness, $H_b$ | 1 |
| Heat sink width, $W$ | 10 | Foot print length of fin, $W_f$ | 0.5-1.5 |
| Fin height, $H_1$ | 0-2 | Foot print width of fin, $W_h$ | 0.5-1.5 |
| Fin height, $H_2$ | 0-2 | Channel width, $W_c$ | 0.6-1.4 |
| Fin height, $H_3$ | 0-2 | Distance between two succesive fins in all directions, $W_b$ | 0.4-1.5 |
| Fin height, $H_4$ | 0-2 | Total number of fins | 48 |
| Side wall width, $W_{sw}$ | 0.5 | Adiabatic section at inlet | 2 |
| Total height of heat sink, $H = H_c + H_b$ | 3 | Adiabatic section at outlet | 2 |

$$\nabla\left(\rho_f \vec{V}\nabla\vec{V}\right) = -\nabla P + \nabla\mu_f\left[\left(\nabla\vec{V} + \nabla\vec{V}^t\right) - \frac{2}{3\nabla\vec{V}}\right] + \rho_f\vec{g} \tag{2}$$

$$\nabla\left[\rho_f C_{p,f}\left(\vec{V}\nabla T\right)\right] = \nabla\left(\lambda_f \nabla T\right) \tag{3}$$

where $\vec{V}$ is the velocity vector, $P$ – the pressure, $T$ – the temperature $\rho_f$, $\mu_f$, $\lambda_f$, $C_{p,f}$, are fluid density, viscosity, thermal conductivity and the specific heat of the coolant, respectively. The superscript, $t$, represents the transpose of a particular matrix and subscript f represents the liquid [13]. For the solid substrate, the continuity equation can be simplify to $\vec{V} = 0$, and energy equation becomes:

$$\lambda_S \nabla^2 T = 0 \tag{4}$$

where $\lambda_S$ is the thermal conductivity of solid substrate. The temperature of the fluid in the micro-channel heat sink is 300 K. The inlet velocity is 0.1 m/s. The bottom of the micro-channel heat sink is heated, and the heat flux density of the heat source is $q_w = 150000$ W/m$^2$.

Commercial code ANSYS 2021R1 has been used where geometries are created on workbench and simulations have been carried out using fluent module for the aforementioned model. Throughout the analysis, the coolant was single-phase liquid water. It is worth mentioning that solid zone of the heat sink retain conduction heat transfer whereas convective mode of heat transfer dominates in the fluid zone as well as solid-liquid interface [13]. Hence, SIMPLEC algorithm is used to deal with the direct coupling of velocity and pressure. In order to improve the accuracy of the calculation results, Residual criteria lower than $10^{-6}$ are considered as convergence for the continuity equation and the momentum conservation equation.

Due to the regular internal structure of micro-channel heat sink, hexahedral grids are used to divide them. Figure 2 shows the meshing used for the simulation of the micro-channel heat sink with pin fins, including fluid zone and solid substrate. In order to identify the accuracy of numerical simulation results and the optimum mesh configuration, grid independence test was done. Table 2 shows the detailed information of the meshing of complete computational domain including both solid and fluid regimes. Figure 3 shows the variation in pressure drop and temperature values with reducing element size. For the first three groups of grids, variation in result is very obvious, but for the last four groups of grids, variation in result is relatively stable as shown in fig. 3. Beyond the grid size of 0.15 mm, the pressure deviation is merely 0.58-1.5% and temperature deviation is merely 0.06-1%. It can be seen that when the grid size

of 0.15 mm has been accurate. Therefore, the grid size of 0.15 mm has been used for the simulation of all configurations of micro-channel heat sink.

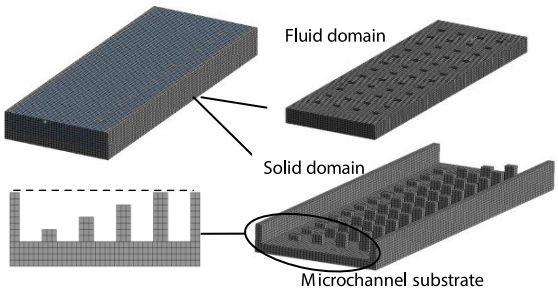


**Figure 2. Meshing of the micro-channel heat sink**

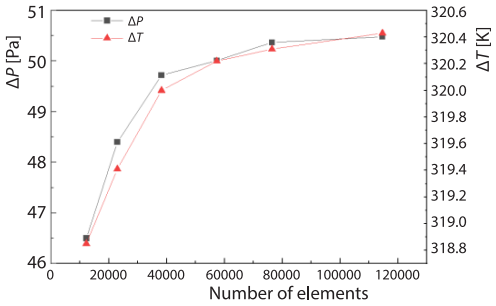


**Figure 3. Variation of pressure drop and temperature with different element size**

**Table 2. Details of mesh size used in grid independence test**

| Element size [mm] | 0.5 | 0.25 | 0.15 | 0.1 | 0.075 | 0.05 |
|---|---|---|---|---|---|---|
| Number of element | 12188 | 22934 | 38223 | 57334 | 76445 | 114667 |

## Optimal design of micro-channel heat sink

### *Optimization of variables and objective functions*

As shown in fig. 4, the design variables are determined as the $W_f$, $W_h$, $H_1$-$H_4$, of the pin fins. Then, the variables, *i.e.*, the $W_f$, $W_h$, and $H_1$-$H_4$, were changed in the range of 0.5-1.5 mm, 0.5-1.5 mm, and 0-2 mm, respectively, to obtain the optimum structure.

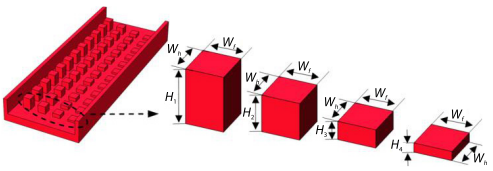

**Figure 4. Front view of the micro-channel heat sink**

Thermal resistance and pumping power are two important indexes to evaluate performance of the micro-channel heat sink. Therefore, the objective functions were established as $R_t$ and $P_p$, which are defined:

$$R_t = \frac{T_{s,max} - T_{f,in}}{qA_s} \tag{5}$$

$$P_p = uNA_{ch}\Delta p \tag{6}$$

where $T_{s,max}$, $T_{f,in}$, $\Delta p$, $u$ are maximum temperature, inlet temperature, pressure drop, and inlet velocity of the micro-channel heat sink, respectively, $q$ – the heat flow density, $A_s$ – the area at the bottom of the micro-channel heat sink, $A_{ch}$ – the cross-sectional area of a single micro-channel while, and $N$ – the total number of micro-channels.

### *Model formation*

Orthogonal experiment is a scientific method to deal with multi-factor and multi-level experiments. Through design of the orthogonal test and orthogonal test results, effective information can be obtained systematically and comprehensively, so as to fit the expressions of the

optimization variables about the two objective functions of thermal resistance and pumping power. In the work, six parameters have been investigated and each parameter has five levels, which are illustrated in tab. 3.

**Table 3. Orthogonal factor and level list**

| Factor | 1 | 2 | 3 | 4 | 5 |
|---|---|---|---|---|---|
| Foot print width of fin $W_h$ [mm] | 0.5 | 0.75 | 1 | 1.25 | 1.5 |
| Foot print length of fin $W_f$ [mm] | 0.5 | 0.75 | 1 | 1.25 | 1.5 |
| Fin height $H_1$ [m] | 0 | 0.5 | 1 | 1.5 | 2 |
| Fin height $H_2$ [mm] | 0 | 0.5 | 1 | 1.5 | 2 |
| Fin height $H_3$ [mm] | 0 | 0.5 | 1 | 1.5 | 2 |
| Fin height $H_4$ [mm] | 0 | 0.5 | 1 | 1.5 | 2 |

The $L_{25}(5^6)$ orthogonal array was adopted to perform the investigation as shown in tab. 4. In the tab. 4, the numbers in the first column are case numbers. Numbers from the second column to the seventh column represent the corresponding levels. It should be noted that the interactions between the factors were ignored in the present work.

**Table 4. The $L_{25}(5^6)$ orthogonal designed scheme and results**

| Case No. | $W_h$ [mm] | $W_f$ [mm] | $H_1$ [mm] | $H_2$ [mm] | $H_3$ [mm] | $H_4$ [mm] | $R_t$ [KW$^{-1}$] | $P_P$ [W] |
|---|---|---|---|---|---|---|---|---|
| 1 | 0.5 | 0.5 | 0 | 0 | 0 | 0 | 0.69135 | $3.37 \cdot 10^{-5}$ |
| 2 | 0.5 | 0.75 | 0.5 | 0.5 | 0.5 | 0.5 | 0.64197 | $4.35 \cdot 10^{-5}$ |
| 3 | 0.5 | 1 | 1 | 1 | 1 | 1 | 0.51851 | $6.71 \cdot 10^{-5}$ |
| 4 | 0.5 | 1.25 | 1.5 | 1.5 | 1.5 | 1.5 | 0.41975 | $9.61 \cdot 10^{-5}$ |
| 5 | 0.5 | 1.5 | 2 | 2 | 2 | 2 | 0.39506 | $10.56 \cdot 10^{-5}$ |
| 6 | 0.75 | 0.5 | 0.5 | 1 | 1.5 | 2 | 0.49382 | $8.95 \cdot 10^{-5}$ |
| 7 | 0.75 | 0.75 | 1 | 1.5 | 2 | 0 | 0.49382 | $8.16 \cdot 10^{-5}$ |
| 8 | 0.75 | 1 | 1.5 | 2 | 0 | 0.5 | 0.49382 | $7.50 \cdot 10^{-5}$ |
| 9 | 0.75 | 1.25 | 2 | 0 | 0.5 | 1 | 0.54321 | $6.49 \cdot 10^{-5}$ |
| 10 | 0.75 | 1.5 | 0 | 0.5 | 1 | 1.5 | 0.54321 | $6.42 \cdot 10^{-5}$ |
| 11 | 1 | 0.5 | 1 | 2 | 0.5 | 1.5 | 0.49382 | $11.10 \cdot 10^{-5}$ |
| 12 | 1 | 0.75 | 1.5 | 0 | 1 | 2 | 0.51851 | $9.95 \cdot 10^{-5}$ |
| 13 | 1 | 1 | 2 | 0.5 | 1.5 | 0 | 0.49382 | $8.71 \cdot 10^{-5}$ |
| 14 | 1 | 1.25 | 0 | 1 | 2 | 0.5 | 0.51851 | $7.45 \cdot 10^{-5}$ |
| 15 | 1 | 1.5 | 0.5 | 1.5 | 0 | 1 | 0.54321 | $7.13 \cdot 10^{-5}$ |
| 16 | 1.25 | 0.5 | 1.5 | 0.5 | 2 | 1 | 0.46913 | $14.35 \cdot 10^{-5}$ |
| 17 | 1.25 | 0.75 | 2 | 1 | 0 | 1.5 | 0.51851 | $12.41 \cdot 10^{-5}$ |
| 18 | 1.25 | 1 | 0 | 1.5 | 0.5 | 2 | 0.49382 | $10.60 \cdot 10^{-5}$ |
| 19 | 1.25 | 1.25 | 0.5 | 2 | 1 | 0 | 0.54321 | $8.72 \cdot 10^{-5}$ |
| 20 | 1.25 | 1.5 | 1 | 0 | 1.5 | 0.5 | 0.54321 | $8.20 \cdot 10^{-5}$ |
| 21 | 1.5 | 0.5 | 2 | 1.5 | 1 | 0.5 | 0.49382 | $19.82 \cdot 10^{-5}$ |
| 22 | 1.5 | 0.75 | 0 | 2 | 1.5 | 1 | 0.49382 | $16.15 \cdot 10^{-5}$ |
| 23 | 1.5 | 1 | 0.5 | 0 | 2 | 1.5 | 0.54321 | $13.71 \cdot 10^{-5}$ |
| 24 | 1.5 | 1.25 | 1 | 0.5 | 0 | 2 | 0.61728 | $10.11 \cdot 10^{-5}$ |
| 25 | 1.5 | 1.5 | 1.5 | 1 | 0.5 | 0 | 0.61728 | $10.00 \cdot 10^{-5}$ |

It can be seen from the data in tab. 4 that the data are discontinuous. Response surface approximation is a method of fitting polynomial function of discrete response and gives the relationship between the objective functions and the design variables [7]. In this paper, the second order polynomial with intercept term, linear term, square term and quadratic interaction term was used as the response function [5]:

$$y(x) = \varphi_0 + \sum_{j=1}^{N} \varphi_j x_j + \sum_{j=1}^{N} \varphi_{jj} x_j^2 + \sum\sum_{i \neq j}^{N} \varphi_j x_j \tag{7}$$

where $x_j$ is the design variable, *i.e.*, $W_f$, $W_h$, and $H_1$-$H_4$, $N$ – the number of design variables, $\varphi$ – the coefficient whose number and can be obtained by $(N+1)(N+2)/2$. In this paper, $N=6$. The number of coefficients is 28, *i.e.*, $a_0$, $a_1 ... a_{27}$ or $b_0$, $b_1 ... b_{27}$.

According to the discrete points and response values in tab. 4, MATLAB multivariate non-linear fitting tool was used, approximate fitting of $R_t$ and $P_p$ was obtained:

$$\begin{aligned} R_t(W_h, W_f, H_1, H_2, H_3, H_4) = {} & a_0 + a_1x_1 + a_2x_2 + x_3x_3 + a_4x_4 + a_5x_5 + a_6x_6 + a_7x_1x_2 + \\ & + a_8x_1x_3 + a_9x_1x_4 + a_{10}x_1x_5 + a_{11}x_1x_6 + a_{12}x_2x_3 + a_{13}x_2x_4 + a_{14}x_2x_5 + \\ & + a_{15}x_2x_6 + a_{16}x_3x_4 + a_{17}x_3x_5 + a_{18}x_3x_6 + a_{19}x_4x_5 + a_{20}x_4x_6 + \\ & + a_{21}x_5x_6 + a_{22}x_1^2 + a_{23}x_2^2 + a_{24}x_3^2 + a_{25}x_4^2 + a_{26}x_5^2 + a_{27}x_6^2 \end{aligned} \tag{8}$$

$$\begin{aligned} P_p(W_h, W_f, H_1, H_2, H_3, H_4) = {} & b_0 + b_1x_1 + x_2x_2 + b_3x_3 + b_4x_4 + b_5x_5 + b_6x_6 + \\ & + b_7x_1x_2 + b_8x_1x_3 + b_9x_1x_4 + b_{10}x_1x_5 + b_{11}x_1x_6 + b_{12}x_2x_3 + b_{13}x_2x_4 + b_{14}x_2x_5 + \\ & + b_{15}x_2x_6 + b_{16}x_3x_4 + b_{17}x_3x_5 + b_{18}x_3x_6 + b_{19}x_4x_5 + b_{20}x_4x_6 + \\ & + b_{21}x_5x_6 + b_{22}x_1^2 + b_{23}x_2^2 + b_{24}x_3^2 + b_{25}x_4^2 + b_{26}x_5^2 + b_{27}x_6^2 \end{aligned} \tag{9}$$

where $x_1$, $x_2$, $x_3$, $x_4$, $x_5$, and $x_6$ are the variables $W_h$, $W_f$, $H_1$, $H_2$, $H_3$, and $H_4$, respectively, and the corresponding coefficients of eqs. (8) and (9) were shown in tab. 5.

**Table 5. Coefficients of objective functions**

| Coefficients | Value | Coefficients | Value | Coefficients | Value | Coefficients | Value |
|---|---|---|---|---|---|---|---|
| $a_0$ | 0.70295 | $a_{14}$ | –0.026152 | $b_0$ | $2.2574 \cdot 10^{-5}$ | $b_{14}$ | $-1.3077 \cdot 10^{-6}$ |
| $a_1$ | 0 | $a_{15}$ | 0.048218 | $b_1$ | 0 | $b_{15}$ | $-7.4128 \cdot 10^{-7}$ |
| $a_2$ | 0 | $a_{16}$ | 0.0027549 | $b_2$ | 0 | $b_{16}$ | $7.1105 \cdot 10^{-6}$ |
| $a_3$ | 0 | $a_{17}$ | –0.021311 | $b_3$ | 0 | $b_{17}$ | $7.8874 \cdot 10^{-6}$ |
| $a_4$ | 0 | $a_{18}$ | 0.027857 | $b_4$ | 0 | $b_{18}$ | $-4.2419 \cdot 10^{-6}$ |
| $a_5$ | 0 | $a_{19}$ | 0.0053667 | $b_5$ | 0 | $b_{19}$ | $8.6372 \cdot 10^{-6}$ |
| $a_6$ | –0.20698 | $a_{20}$ | 0.01121 | $b_6$ | $4.9303 \cdot 10^{-5}$ | $b_{20}$ | $-3.4965 \cdot 10^{-6}$ |
| $a_7$ | 0 | $a_{21}$ | 0.022436 | $b_7$ | 0 | $b_{21}$ | $6.3533 \cdot 10^{-6}$ |
| $a_8$ | 0 | $a_{22}$ | 0.02107 | $b_8$ | 0 | $b_{22}$ | $3.7956 \cdot 10^{-5}$ |
| $a_9$ | 0 | $a_{23}$ | –0.0053481 | $b_9$ | 0 | $b_{23}$ | $-5.8282 \cdot 10^{-6}$ |
| $a_{10}$ | 0 | $a_{24}$ | –0.02735 | $b_{10}$ | 0 | $b_{24}$ | $9.5722 \cdot 10^{-6}$ |
| $a_{11}$ | 0 | $a_{25}$ | –0.020294 | $b_{11}$ | 0 | $b_{25}$ | $2.2616 \cdot 10^{-6}$ |
| $a_{12}$ | 0.011818 | $a_{26}$ | –0.014862 | $b_{12}$ | $-1.528 \cdot 10^{-5}$ | $b_{26}$ | $-3.4851 \cdot 10^{-6}$ |
| $a_{13}$ | –0.025164 | $a_{27}$ | 0.032331 | $b_{13}$ | $-2.3743 \cdot 10^{-6}$ | $b_{27}$ | $-1.7918 \cdot 10^{-6}$ |

Moreover, the root mean square error (RMSE), sum of squared error (SSE), and multivariate statistical coefficient, $R^2$, are used to verify the accuracy of the objective functions fitting equations and are defined [19]:

$$RMSE = \sqrt{\frac{1}{m}\sum_{i=1}^{m}(h_i - y_i)^2} \tag{10}$$

$$SSE = \sum_{i=1}^{m}(h_i - y_i)^2 \tag{11}$$

$$R^2 = 1 - \frac{\sum_{i=1}^{m}(h_i - y_i)^2}{\sum_{i=1}^{m}(h_i)^2} \tag{12}$$

where $h_i$, $y_i$, and $m$ are the numerical data, the predicted data, and the number of data sets, respectively. Equation (12) suggests that objective functions can meet the accuracy requirement if $0.9 < R^2 < 1$.

By solving eqs. (10)-(12), the values obtained for RMSE, SSE, and $R^2$ are 0.0223, 0.0035, and 0.965, respectively for the thermal resistance function, and $65024 \cdot 10^{-6}$, $2.9597 \cdot 10^{-10}$, and 0.991, respectively for the pumping power function, which were shown in tab. 6. This shows that they can accurately predict values of $R_t$ and $P_p$.

**Table 6. Performance evaluation index of prediction equations of $R_t$ and $P_P$**

| Objective functions | RMSE | SSE | $R^2$ |
|---|---|---|---|
| $R_t$ | 0.0223 | 0.0035 | 0.965 |
| $P_p$ | $65024 \cdot 10^{-6}$ | $2.9597 \cdot 10^{-10}$ | 0.991 |

### *Multi-objective genetic optimization*

In engineering applications, it is very difficult in most cases to satisfy all the planned or required objectives. Generally, the improvement of the performance of one target will cause to the decline of the performance of another or more targets. With the change of structural parameters of pin fins in micro-channel heat sink, the influence on thermal resistance and pump power are conflicting and contradictory. Therefore, it is necessary to co-ordinate and trade off according to the proportion of different sub objectives, so that each sub objective can be met as closely as possible. Then, NGSA-II was selected as the multi-objective optimization algorithm with advantage of fast non-dominated sorting approach. The *k*-means clustering was used to cluster the Pareto optimal solution based on the minimum distance method for classifying the samples and obtaining representative solutions. Hence, the combination of NSGA-II genetic algorithm and *k*-means cluster analysis was applied to the optimal design of the structural parameters of the pin fins in the micro-channel heat sink, so as to select the optimal combination of the structural parameters of the pin fins that can achieve the optimal thermal resistance and pumping power.

Thermal resistance and pumping power are objective functions. The multi-objective optimization model can be described:

$$\begin{gathered}\min f\left(W_{\mathrm{h}}, W_{\mathrm{f}}, H_1, H_2, H_3, H_4\right)= \\ =\min\left\{R_{\mathrm{t}}\left(W_{\mathrm{h}}, W_{\mathrm{f}}, H_1, H_2, H_3, H_4\right), P_{\mathrm{p}}\left(W_{\mathrm{h}}, W_{\mathrm{f}}, H_1, H_2, H_3, H_4\right)\right\} \\ \text{s.t} \quad 0.5 < W_{\mathrm{h}} < 1.5 \ \text{mm} \\ 0.5 < W_{\mathrm{f}} < 1.5 \ \text{mm} \\ 0 < H_1 < 2 \ \text{mm} \\ 0 < H_2 < 2 \ \text{mm} \\ 0 < H_3 < 2 \ \text{mm} \\ 0 < H_4 < 2 \ \text{mm} \\ u_{\mathrm{in}} = 0.1 \ \text{m/s}\end{gathered} \tag{13}$$

In the work, the NSGA-II algorithm program in MATLAB is used to simulate the aforementioned model, and the thermal resistance and pumping power are calculated. In all algorithm calculations, the population size, probabilities of crossover, and mutation are set as 100, 0.9, and 0.25, respectively. After 2000 steps of iterative calculation, the Pareto optimal solution set is obtained, as shown in fig. 5. The experimental results show that the objective functions of thermal resistance and pumping power are opposite. When one objective function is improved, the other objective function becomes worse. For each fixed value of one objective function, there is an optimal value for the other objective function.

### *The k-means clustering analysis*

For the multi-objective optimization design problem, the Pareto optimal solution is not unique, but multiple solutions constitute the Pareto optimal solution set. The *k*-means clustering was used to cluster the Pareto optimal solution of the previous model to find five representative solutions in the solution set. The five representative solutions and corresponding variables are shown in tab. 7.

**Table 7. Five representative solutions and the design values of corresponding variables**

| Clustering point | $W_{\mathrm{h}}$ [mm] | $W_{\mathrm{f}}$ [mm] | $H_1$ [mm] | $H_2$ [mm] | $H_3$ [mm] | $H_4$ [mm] | $R_{\mathrm{t}}$ [KW$^{-1}$] | $P_{\mathrm{P}}$ [W] |
|---|---|---|---|---|---|---|---|---|
| A | 0.7450 | 1.4999 | 1.9891 | 0.3716 | 2.0000 | 0.2410 | 0.3964 | $5.8283 \cdot 10^{-5}$ |
| B | 0.8005 | 1.4986 | 1.9052 | 0.0125 | 1.9999 | 0.0088 | 0.4193 | $3.7922 \cdot 10^{-5}$ |
| C | 0.8004 | 1.4990 | 1.7184 | 0.0043 | 1.9999 | 0.0043 | 0.4428 | $3.2289 \cdot 10^{-5}$ |
| D | 0.8003 | 1.4999 | 1.3752 | 0.0123 | 2.0000 | 0.0114 | 0.4797 | $2.5102 \cdot 10^{-5}$ |
| E | 0.8004 | 1.4996 | 0.6614 | 0.0003 | 2.0000 | 0.0017 | 0.5380 | $1.5491 \cdot 10^{-5}$ |

## Results and discussion

Figure 5 shows that multi-objective optimization is realized based on NSGA-II genetic algorithm in MATLAB to obtain the Pareto optimization solution set. Figure 6 shows the Pareto front calculated by the NSGA-II algorithm and five clustering points obtained by the *k*-means clustering which are A, B, C, D, and E, respectively. Figure 6 also shows that the Pareto front is divided into six regions delimited by five clustering points. A low thermal resistance is accompanied by a high pumping power or *vs*. The thermal resistance at A is 0.74 times that at E, but the pumping power at A is 3.76 times that at E. The thermal resistance at E

is 1.36 times that at A, but the pumping power at E is 0.27 times that at A. It is clearly that the improvement of one parameter always comes at the expense of the other. Region 1 displays the lowest thermal resistance and the highest pumping power while regions 2-5 show moderate thermal resistance and pumping power. Region 6 starts just after the point E, which is opposite to the phenomenon of Region 1, namely, the highest thermal resistance and the lowest pumping power. Therefore, there is an effective trade-off point between A and E, and the designer can select the appropriate parameter combination according to the actual needs.

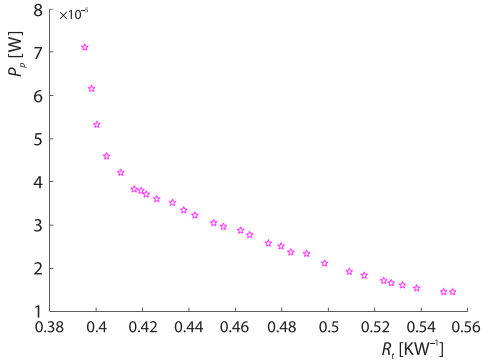


**Figure 5. Pareto front of thermal resistance and pumping power**

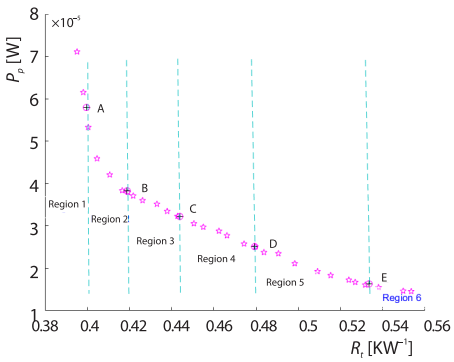


**Figure 6. The *k*-means clustering of Pareto optimal solution of thermal resistance and pumping power**

Comparison and verification of simulation experiment results are shown in tab. 8. In order to ensure grid division, the experimental data in tab. 8 retain two significant digits. It compared three different cases: before optimization, after optimization (five representative solutions) and Bhandari *et al.* [13] model, respectively. The nephogram of temperature field and pressure distribution for them as show figs. 7(a)-7(c).

**Table 8. Comparison and verification of simulation experiments**

| CASE | | $W_h$ [mm] | $W_f$ [mm] | $H_1$ [mm] | $H_2$ [mm] | $H_3$ [mm] | $H_4$ [mm] | $T$ [K] | $\Delta p$ [Pa] |
|---|---|---|---|---|---|---|---|---|---|
| [13] | | 1.00 | 1.00 | 1.50 | 1.50 | 1.50 | 1.50 | 315.4 | 112.3 |
| Before optimization | | 1.50 | 0.50 | 2.00 | 1.50 | 1.00 | 0.50 | 320.4 | 131.8 |
| After optimization | Case A | 0.76 | 1.50 | 1.99 | 0.37 | 2.00 | 0.24 | 314.0 | 115.7 |
| | Case B | 0.80 | 1.50 | 1.91 | 0.01 | 2.00 | 0.01 | 314.8 | 84.4 |
| | Case C | 0.80 | 1.50 | 1.72 | 0.00 | 2.01 | 0.00 | 315.4 | 64.4 |
| | Case D | 0.80 | 1.50 | 1.38 | 0.01 | 2.00 | 0.01 | 316.0 | 56.4 |
| | Case E | 0.80 | 1.50 | 0.66 | 0.00 | 2.00 | 0.00 | 317.0 | 50.9 |

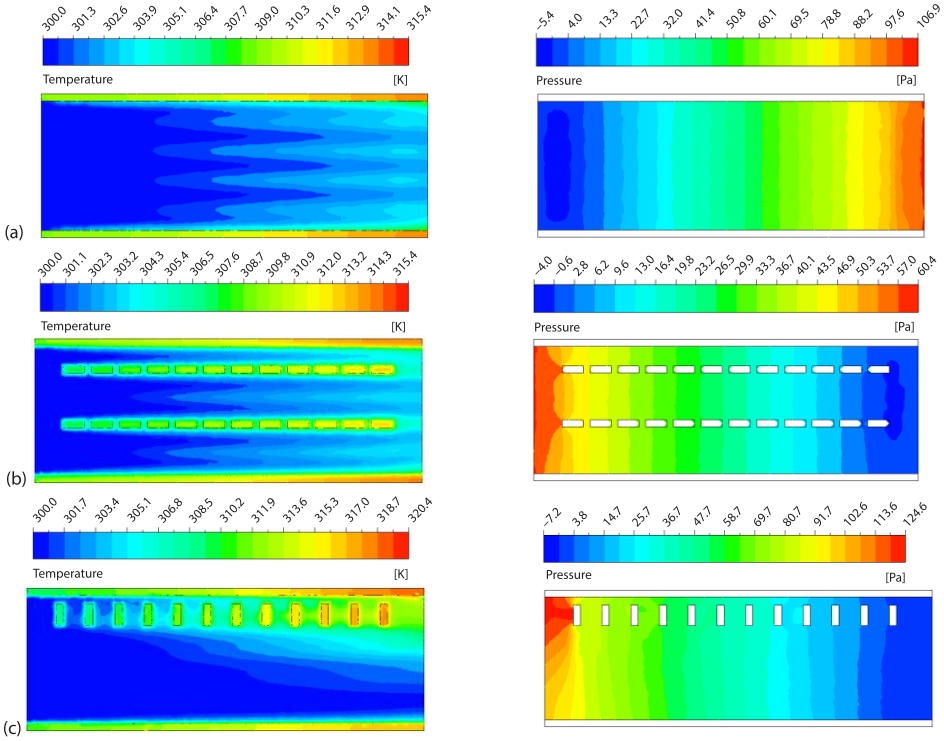


**Figure 7. Nephogram of temperature field and pressure distribution; (a) for [13], (b) for Case C, and (c) before optimization**

The effect of enhanced heat transfer efficiency and flow resistance should be considered comprehensively. The experimental results show that the heat transfer performance of micro-channel heat sink is improved, and the flow resistance is also increased, which means that the thermal resistance is reduced and the pumping power is increased. Therefore, it is necessary to synthesize the reference factors of enhanced heat transfer efficiency and flow resistance to evaluate the comprehensive heat transfer performance of micro-channels heat sink before and after optimization, namely, enhanced heat transfer evaluation factor $\eta$:

$$\mathrm{Nu} = \frac{hD_\mathrm{h}}{\lambda_\mathrm{f}} \tag{14}$$

$$h = \frac{Q}{NA_\mathrm{ch}\Delta T} = \frac{qA_\mathrm{s}}{NA_\mathrm{ch}\left(T_\mathrm{s} - T_\mathrm{f}\right)} \tag{15}$$

$$f = \frac{2\Delta p D_\mathrm{h}}{\rho_\mathrm{f} L_\mathrm{ab} u^2} \tag{16}$$

$$\eta = \frac{\dfrac{\mathrm{Nu}}{\mathrm{Nu}_0}}{\left(\dfrac{f}{f_0}\right)^{1/3}} \tag{17}$$

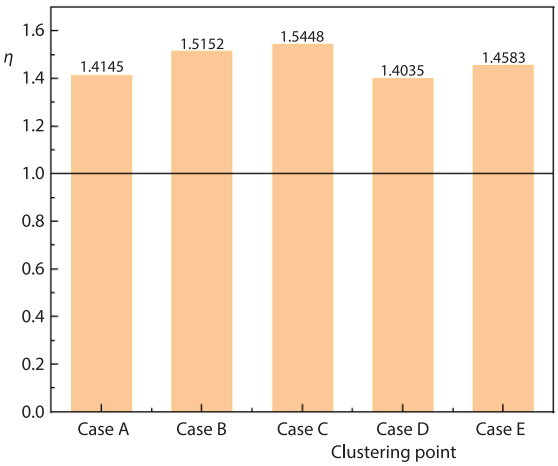


**Figure 8. Variations of $\eta$ for five cases**

where Nu is the Nussert number, $D_h$ – the hydraulic diameter of micro-channel heat sink, $h$ – the heat transfer coefficient, $T_s$ – the average temperature of the heated bottom, $T_f$ – the average temperature of the fluid, $L_{ab}$ – the length of micro-channel heat sink, and $f$ – the parameter $f$is the friction coefficient of the micro-channel heat sink. Subscript 0 indicates before optimization. Figure 8 illustrates the enhanced heat transfer evaluation factor for the optimized micro-channel heat sink. As shown fig. 8, the enhanced heat transfer evaluation factor is higher than 1 for all cases, which proves that the optimized micro-channel heat sink can improve the heat transfer performance. The enhanced heat transfer evaluation factor are 1.4145, 1.5152, 1.5448, 1.4035, and 1.4583 for the optimized (Case A to Case E) micro-channel heat sink, respectively. The maximum the enhanced heat transfer evaluation factor at $C$ is 1.5448, so the comprehensive heat transfer performance of this group is the best.

Comparing Case C with Bhandari *et al.* [13] model, it is found that the maximum temperature of micro-channel heat sink is the same, but the pressure drop of Case C is reduced by 42.7%. Moreover, Comparing Case C with before optimization, it is found that the maximum temperature of micro-channel heat sink and the pressure drop of case C is reduced by 1.6 % and 51.1 %, respectively.

## Conclusion

This paper presents a new structure of open rectangular micro-channel heat sink with pin fins was proposed to enhance heat transfer. A multi-objective optimization using orthogonal test method, NSGA-II, and $k$-mean clustering was performed. The experiment results show that there are effective tradeoff points between the highest and lowest points of the five clustering points (Case A to case E) which can make both the pumping power and thermal resistance within the optimal range, so as to obtain the optimal micro-channel heat sink. Hence, the optimal parameter design of micro-channel heat sink can be obtained through multi-objective optimization improve the comprehensive heat transfer performance of micro-channel heat sink.

## Acknowledgment

This work was supported by Guangzhou Science and Technology Project (201904010107), Guangdong Provincial Natural Science Foundation of China (2019A151 5010793), Guangdong Province Science and Technology Project (2016B090918071).

## References

[1] Rakesh, B., *et al.*, Simplistic Approach to Reduce Thermal Issues in 3-D IC Integration Technology, *Materials Today:Proceedings*, *45* (2021), 2, pp. 1399-1402
[2] Bin, D., *et al.*, Coupling Management Optimization of Temperature and Thermal Stress Inside 3-D-IC with Multi-cores and Various Power Density, *International Communications in Heat and Mass Transfer*, *120* (2021), 105021

[3] Bin, D., *et al.*, A Novel Thermal Management Scheme for 3D-IC Chips with Multi-Cores and High Power Density, *Applied Thermal Engineering*, *168* (2020), 114832
[4] Wang, K.-J., *et al.*, Thermal Management of 3-D Integrated Circuits with Special Structures, *Thermal Science*, *25* (2021), 3B, pp. 2221-2225
[5] Shi, X. J., *et al.*, Multi-Objective Optimization on the Geometrical Parameters of a Nanofluid-Cooled Rectangular Micro-Channel Heat Sink, *Journal of Xi 'an Jiaotong University, 52* (2018), 5, pp. 56-61
[6] Salvi, S. S., *et al.*, A Review of Recent Research on Heat Transfer in 3-D Integrated Circuits (3-D IC), *IEEE Transactions on Components, Packaging & Manufacturing Technology*, *11* (2021), 5, pp. 802-821
[7] Peitao, Y., *et al.*, Thermal Performance Analysis of Multi-objective Optimized Micro-Channels with Triangular Cavity and Rib Based on Field Synergy Principle, *Case Studies in Thermal Engineering, 25* (2021), 100963
[8] Zeng, L., *et al.* Thermal and Flow Performance in Micro-Channel Heat Sink with Open-Ring Pin Fins, *International Journal of Mechanical Sciences*, *200* (2021), 106445
[9] Chai L, *et al.*, Numerical Simulation of Fluid-Flow and Heat Transfer in a Micro-Channel Heat Sink with Offset Fan-Shaped Reentrant Cavities in Sidewall, *International Communications in Heat and Mass Transfer*, *38* (2011), 5, pp. 577-584
[10] Xia, G. D., *et al.*, Numerical Investigation of Thermal Enhancement in a Micro Heat Sink with Fan-shaped Reentrant Cavities and Internal Ribs, *Applied Thermal Engineering*, *58* (2013), 1-2, pp. 52-60
[11] Hong, F., *et al.*, The 3-D Numerical Analyses and Optimization of Offset Strip-Fin Micro-Channel Heat Sinks, *International Communications in Heat and Mass Transfer*, *36* (2009), 7, pp. 651-656
[12] Yadav, V., *et al.*, Numerical Investigation of Heat Transfer in Extended Surface Micro-channels, *International Journal of Heat and Mass Transfer*, *93* (2016), Feb., pp. 612-622
[13] Bhandari, P., *et al.*, Thermal Performance of Open Micro-channel Heat Sink with Variable Pin Fin Height, *International Journal of Thermal Sciences*, *159* (2021), 106609
[14] Husain, A., *et al.*, Optimization of a Micro-channel Heat Sink with Temperature Dependent Fluid Properties, *Applied Thermal Engineering, 28* (2008), 8, pp. 1101-1107
[15] Adham, A. M., *et al.*, Optimization of Nanofluid-Cooled Micro-Channel Heat Sink*, Thermal Science, 20* (2016), 1, pp. 109-118
[16] Vinoth, *et al.*, Numerical Study of Inlet Cross-section Effect on Oblique Finned Micro-Channel Heat Sink, *Thermal Science, 22* (2018), 6, pp. 2747-2757
[17] Kulkarni, K., *et al.*, Multi-Objective Optimization of a Double-Layered Micro-Channel Heat Sink with Temperature-Dependent Fluid Properties, *Applied Thermal Engineering*, *99* (2016), 1, pp. 262-272
[18] Prajapati, Y. K., *et al.*, Influence of Fin Height on Heat Transfer and Fluid-Flow Characteristics of Rectangular Micro-Channel Heat Sink, *International Journal of Heat & Mass Transfer, 137* (2019), July, pp. 1041-1052
[19] Wang, J., *et al.*, Structural Optimization of Micro-Channels Based on Multi-objective Genetic Algorithm, *Journal of Chemical Engineering of Chinese Universities, 34* (2020), 4, pp. 1034-1043

Paper submitted: October 23, 2021
Paper revised: December 31, 2021
Paper accepted: January 3, 2022